Journal of Luminescence 148 (2014) 151–155

Contents lists available at ScienceDirect

Journal of Luminescence

journal homepage: www.elsevier.com/locate/jlumin

Anomalous luminescence from Yb^{2+}-doped Ca_2PO_4Cl

De-Yin Wang [a], Yi-Chen Chiu [b], Chien-Hao Huang [b], Yun-Chen Wu [a], Teng-Ming Chen [a,*]

[a] Phosphors Research Laboratory and Department of Applied Chemistry, National Chiao Tung University, Hsinchu 30010, Taiwan
[b] Material and Chemical Research Laboratories, Industrial Technology Research Institute, Chutung 31040, Taiwan

ARTICLE INFO

Article history:
Received 19 April 2013
Received in revised form
1 November 2013
Accepted 24 November 2013
Available online 17 December 2013

Keywords:
Luminescence
$Ca_2PO_4Cl:Yb^{2+}$
Trapped-exciton state
Temperature-dependent luminescence

ABSTRACT

The photoluminescence of $Ca_2PO_4Cl:Yb^{2+}$ has been investigated and compared with that of $Ca_2PO_4Cl:Eu^{2+}$, and the application of $Ca_2PO_4Cl:Yb^{2+}$ for white LED has been evaluated. The excitation spectra of $Ca_2PO_4Cl:Yb^{2+}$ are dominated by an intense excitation band at 395 nm. Under near-UV excitation at 395 nm, $Ca_2PO_4Cl:Yb^{2+}$ shows a broad asymmetric emission with maximum at 490 nm. This emissions result from two different Yb^{2+} centers is evidenced by the low temperature ($T=100$ K) emission spectrum. Yb^{2+} luminescence differs significantly from that of Eu^{2+}, most notably in the structure of emission spectra, and is characterized by a much broader emission band and lower quenching temperature. Such anomalous luminescence from Yb^{2+} is ascribed to the de-excitation process of the Yb^{2+}-trapped exciton state. $Ca_2PO_4Cl:Yb^{2+}$ has external quantum efficiency of 24% and exhibits 40% of luminescence quenching at 100 °C in the air and, therefore, these results reveal its limited potential in the fabrication of white-light LEDs.

1. Introduction

White light-emitting diodes (LEDs) are considered as the next generation of lighting source after incandescent and fluorescent lamps [1–13]. In comparison with incandescent and fluorescent lamps, the use of white-light LEDs is advantageous due to long life, low power consumption, and minimal maintenance. White light in LEDs is commonly produced by two different ways: one is combining blue LED chip with a yellow-emitting $Y_3Al_5O_{12}:Ce^{3+}$ garnet phosphor, and the other is combining near ultraviolet (*n*-UV) LED chip with RGB phosphors. Both methods of obtaining white light require the use of phosphors, which undoubtedly play an important role in generating high-quality white light. Accordingly, with the development of the white LED industry, the search for new phosphors used for the conversion of the *n*-UV to blue emission from (In,Ga)N LEDs into visible light has rapidly increasing [1–13]. Eu^{2+} has been commonly used as the luminescent center for phosphors. This is due to the ion's 4f–5d transition which is parity-allowed, and the involved 5d states are highly sensitive to their chemical surrounding. As a result, doping Eu^{2+} in certain host matrices can lead to strong absorption in the *n*-UV to blue spectral range combined with efficient emission in the visible range. Similar to the Eu^{2+} ion, the Yb^{2+} ion can be stabilized in the divalent charge state in solids because they have stable $4f^7$ (half-filled) and $4f^{14}$ (completely-filled) configurations, and give 5d–4f emission. However, unlike the luminescence of Eu^{2+}, few reports in the literature are available regarding the case of Yb^{2+} luminescence. Recently, the luminescence of some Yb^{2+} activated compounds has been studied. Yoo et al. described the photoluminescence properties of Yb^{2+}-doped $Ba_5(PO_4)_3Cl$ and proposed its application in white-light LED [14]. Huang et al. reported the luminescence of $NaBaPO_4:Yb^{2+}$ and discovered that the luminescence decay of $NaBaPO_4:Yb^{2+}$ shows typical decay times for impurity (Yb^{2+})-trapped exciton emission [15]. Yb^{2+} doped CaAlSiN$_3$ and beta-SiAlON have been suggested as novel red-emitting and green-emitting phosphor for white LEDs [16,17], respectively.

In our previous work, observations have been made suggesting Eu^{2+} could produce efficient blue emission in Ca_2PO_4Cl with intensity even stronger than that of the commercial blue-emitting phosphor, $BaMgAl_{10}O_{17}:Eu^{2+}$ (BAM), under *n*-UV excitation [13]. Moreover, Yb^{2+} ion was observed to show similar or slightly red-shift wavelength emission than that of Eu^{2+} in the same host lattices [18]. Therefore, efficient emission from Yb^{2+} is expected in Ca_2PO_4Cl. In order to examine other possible phosphors used in white LEDs, in this paper, we investigate the luminescence properties of Yb^{2+} in Ca_2PO_4Cl, and compare the luminescence properties of Yb^{2+} with those of Eu^{2+} in the same host matrix.

2. Experimental section

2.1. Materials and synthesis

Powder samples of Yb^{2+}- and Eu^{2+}-doped Ca_2PO_4Cl were synthesized by the solid-state reaction method. The starting materials are as follows: $CaCO_3$ ($\geq$99.0%, Aldrich), anhydrous $CaCl_2$ ($\geq$99.0%, Aldrich), $(NH_4)_2HPO_4$ (99.9%, Aldrich), Yb_2O_3

* Corresponding author.
E-mail address: tmchen@mail.nctu.edu.tw (T.-M. Chen).

0022-2313/$ - see front matter © 2013 Elsevier B.V. All rights reserved.
http://dx.doi.org/10.1016/j.jlumin.2013.11.082

(99.99%, Grirem) and Eu_2O_3 (99.99%, Grirem). All starting materials were weighed in stoichiometric proportions with the exception of $CaCl_2 \cdot 2H_2O$ which was in excess of ~2 wt%. The materials were then ground in a glove box. The obtained mixtures were sintered under a reducing atmosphere (40%H_2:60%Ar) at 850 °C for 6 h and allowed to cool at room temperature. The obtained products were washed with deionized water for 3–4 times to remove excess $CaCl_2$ and then dried at 100 °C in an oven overnight for further measurements.

2.2. Characterizations

The phase purity of all samples was verified using powder X-ray diffraction (XRD) analysis with a Bruker AXS D8 Advanced Automatic Diffractometer operated at 40 kV and 40 mA with Cu Kα radiation ($\lambda = 1.5418$ Å). The photoluminescence (PL) and PL excitation (PLE) spectra of the samples were measured by using a Spex Fluorolog-3 spectrofluorometer (HORIBA Jobin-Yvon, Inc.) equipped with a 450 W Xe light source. Thermal quenching of luminescence of phosphors was investigated using a THMS-600 heating apparatus attached to the Spex Fluorolog-3 spectrofluorometer.

3. Results and discussion

3.1. Phase identification

The XRD patterns of Yb^{2+}-doped Ca_2PO_4Cl with various dopant contents are shown in Fig. 1. The XRD patterns of the synthesized Ca_2PO_4Cl:xYb^{2+} with low Yb^{2+} doping concentrations are in good agreement with that reported in PDF no. 190247, indicating the compound retained the same crystal structure as Ca_2PO_4Cl. However, when Yb^{2+} doping concentration is increased to 4%, some apparent extra peaks attributed to Yb_2O_3 appear, and the diffraction intensity corresponding to the Yb_2O_3 phase increases with further increasing the Yb^{2+} doping content, suggesting the solubility of Yb^{2+} in $Ca_{2-x}Yb_xPO_4Cl$ is low.

3.2. Spectroscopic characterizations and comparison between Ca_2PO_4Cl:Yb^{2+} and Ca_2PO_4Cl:Eu^{2+}

In the whole concentration range of Yb^{2+} doping, the PL and PLE spectra of Ca_2PO_4Cl:xYb^{2+} ($1\% \le x \le 5\%$) are the same except intensity. As a reference, Fig. 2 presents the PL and PLE spectra of the 2% Yb-doped Ca_2PO_4Cl. The PLE spectrum of Ca_2PO_4Cl:Yb^{2+} is composed of a number of bands with peaks at 275 nm, 316 nm and 395 nm, which are due to the crystal splitting of 5d state. Upon excitation of

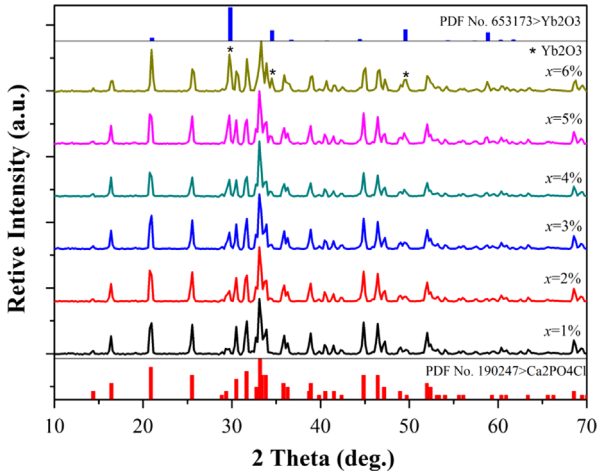

Fig. 1. XRD patterns of Ca_2PO_4Cl:xYb^{2+} ($1\% \le x \le 6\%$).

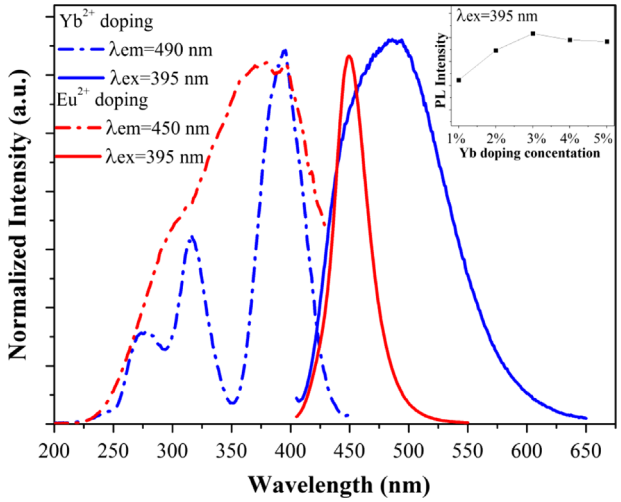

Fig. 2. PL and PLE spectra of Ca_2PO_4Cl:2%Yb^{2+} and Ca_2PO_4Cl:2%Eu^{2+}. The inset shows the dependence of PL intensity of Ca_2PO_4Cl:xYb^{2+} on Yb^{2+} doping concentration (x) under 395 nm excitation.

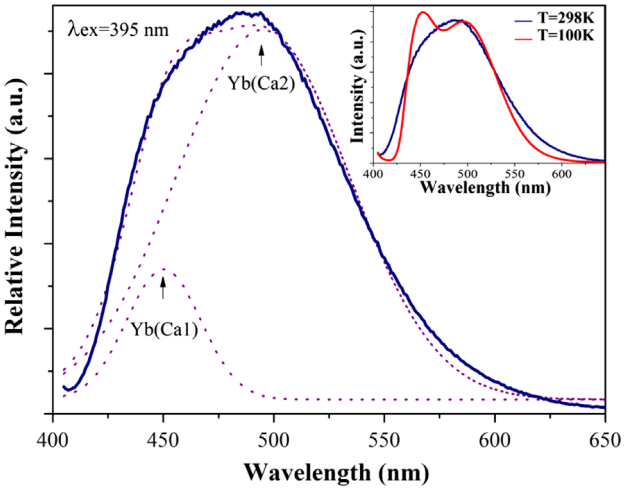

Fig. 3. The representative PL spectrum of Ca_2PO_4Cl:2%Yb^{2+} given by Gaussian fit into two components at 450 and 495 nm, respectively. The inset shows the PL spectra measured at room temperature and low temperature at 100 K. The two emission spectra are normalized on the intensity of the emission band at 495 nm.

Yb^{2+} into its 5d state at 395 nm, the PL spectrum shows (1) a broad asymmetric band with maximum centered at 490 nm and (2) full width at half maximum (FWHM) of about 110 nm (~4640 cm^{-1}). The inset in Fig. 2 shows the dependence of Yb^{2+} emission intensity on its doping concentration (x) in Ca_2PO_4Cl:Yb^{2+} and the optimal Yb^{2+} concentration was found to be 3%. For more than 3%, Yb^{2+} emission starts to decrease due to concentration quenching effect. Using a Gaussian fit, the asymmetric PL spectrum of Ca_2PO_4Cl:Yb^{2+} can be fitted into two Gaussian bands with peaks at 450 nm with FWHM about 40 nm (1942 cm^{-1}) and 495 nm with FWHM about 95 nm (4005 cm^{-1}) (see Fig. 3), respectively. The fitted peaks correspond to the emission from two different Yb^{2+} centers. A preliminary Ca_2PO_4Cl structural study shows that there are two different crystallographic sites available for the divalent Ca^{2+} ions: a larger site with C_2 symmetry noted as Ca1, and a smaller site with C_S symmetry noted as Ca2 [13,20]. At both sites, Ca^{2+} is coordinated by six O^{2-} ions and two Cl^- ions. For the relatively larger Ca1 site, the average Ca–O distance is 2.50 Å and the average Ca–Cl distance is 2.89 Å. For the relatively smaller Ca2 site, the corresponding distances are 2.46 Å and 2.81 Å, respectively [13,20]. In similar coordination environments, the crystal field splitting of the 5d state depends on the distance between

the central ions and the ligands (R) and is proportional to R^{-5} [21]. As a consequence, the lowest 5d state will move downward in energy with the increasing crystal-field splitting, and its position would change greatly even with a slight change of distance (R) [21]. Therefore, the emission band at 450 nm is assigned to emission originates from Yb^{2+} at the larger Ca1 site and noted as Yb(Ca1), while the emission band at 495 nm results from Yb^{2+} at the smaller Ca2 site and noted as Yb(Ca2). In addition, we measured the PL spectrum of the same Yb^{2+}-doped sample at 100 K and presented the results in the inset of Fig. 3. Due to a decrease of the electron–lattice phonon interaction at low temperature, accompanied by the decrease of emission band width, the PL spectrum becomes well resolved into two bands at 100 K with peaks close to the fitted Gaussian bands previously described. These findings further confirm the asymmetric nature of the PL spectrum at room temperature results from two different Yb^{2+} emission centers. The emission intensity from Yb^{2+} (Ca1) at room temperature is largely reduced compared to that at $T=100$ K, presumably caused by the thermal assisted energy transfer from Yb^{2+} (Ca1) to Yb^{2+} (Ca2).

In the meantime, we have compared the luminescence of Yb^{2+} in Ca_2PO_4Cl with that of Eu^{2+} in Ca_2PO_4Cl. The PL and PLE spectra of 2% Eu^{2+}-doped Ca_2PO_4Cl sample were also shown in Fig. 2, and their PL and PLE intensities are normalized with that of Yb^{2+}-doped sample. When comparing with the PL and PLE spectra of Yb^{2+} with those of Eu^{2+} in Ca_2PO_4Cl:Eu^{2+}, we find that: (1) although the lowest energy f–d excitation band of Yb^{2+} is close to that of Eu^{2+}, the PLE spectrum of Yb^{2+} shows fine structure unlike Eu^{2+}, which is partially due to the less complex electron structure of Yb^{2+} in comparison with that of Eu^{2+} [19]; (2) the Yb^{2+} emission is obviously red-shifted with emission maximum at 490 nm versus that at 450 nm for Eu^{2+}. In the meantime, the Yb^{2+} emission band is much broader than that of Eu^{2+} (FWHM=110 nm for Yb^{2+} versus FWHM=35 nm for Eu^{2+}). This type of anomalous emission has been observed in other studies on Yb^{2+}-doped matrix hosts [22–24], such as SrF_2 [22], $SrSi_2O_2N_2$ [23] and $SrSi_2AlO_2N_3$ [24]. The emission has been attributed to an impurity (Yb^{2+})-trapped exciton state [22–24] that has been confirmed by photoconductivity experiments in the case of SrF_2:Yb^{2+} [22]. In these models, it is emphasized that the anomalous emission from Yb^{2+} can only be observed when its lowest 5d state is located in the conduction band [22–24]. Upon 4f–5d excitation, one electron of Yb^{2+} will be pumped from 4f state to 5d state leaving a hole in its 4f state. Due to the energy position overlap between the 5d state of Yb^{2+} and the conduction band of the host, the excited electron will become delocalized through photoionization and results in the formation of [Yb^{3+}], which can be viewed as a state that Yb^{2+} is bound with a hole. The excited electrons can be captured in electron traps and be delocalized in the surrounding area of the excited [Yb^{3+}], giving rise to (Yb)-trapped exciton state. Subsequent recombination of the delocalized electron on surrounding [Yb^{3+}] ions with the hole localized on the photoionized [Yb^{3+}] ion will generate a (Yb)-trapped exciton emission. In comparison with Eu^{2+} emission in Ca_2PO_4Cl, Yb^{2+} emission is indeed different and anomalous. Using Ca_2PO_4Cl as a host, we observe similar behavior to what was observed in SrF_2, $SrSi_2O_2N_2$ and $SrSi_2AlO_2N_3$ [22–24], suggesting a similar origin of anomalous emission of Yb^{2+} in Ca_2PO_4Cl, viz., from recombination of the excited (Yb)-trapped exciton.

To explain the observed anomalous Yb^{2+} emission in Ca_2PO_4Cl, we have proposed that in the same host, the lowest 5d state of Yb^{2+} is located within the conduction band, whereas that of Eu^{2+} is located below the conduction band, as indicated in Fig. 4. The anomalous Yb^{2+} emission has been attributed to the de-excitation of an impurity (Yb)-trapped exciton state. In the host of Ca_2PO_4Cl, there are two Ca^{2+} sites available for Yb^{2+}, which were noted as larger Ca1 site and smaller Ca2 site. When Yb^{2+} substitutes Ca^{2+} ions, it will produce two different Yb^{2+}-trapped exciton states. The emission band at 450 nm is from the de-excitation of the Yb^{2+}-trapped exciton state with a higher energy while the emission band at 495 nm results from the de-excitation of the Yb^{2+}-trapped exciton state with a lower energy.

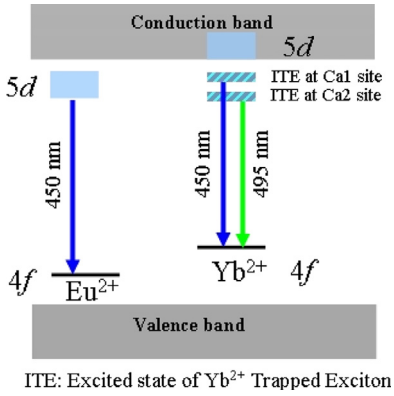

Fig. 4. Proposed energy level diagram of Eu^{2+} and Yb^{2+} in the Ca_2PO_4Cl host for explaining the anomalous Yb^{2+} emission.

3.3. Comparison of temperature-dependent luminescence between Ca_2PO_4Cl:Yb^{2+} and Ca_2PO_4Cl:Eu^{2+}

To further evaluate the luminescence properties of Yb^{2+}, we have examined its thermal luminescence quenching behavior and compared the results with that of Ca_2PO_4Cl:Eu^{2+}. Fig. 5(a) and (b) shows the temperature dependence of PL intensity for Ca_2PO_4Cl:2%Yb^{2+} and Ca_2PO_4Cl:2%Eu^{2+}, respectively. Throughout the range of temperature studied, the Yb^{2+}-doped sample shows a much inferior thermal stability than the Eu^{2+} doped sample, which limits Ca_2PO_4Cl:Yb^{2+} to be used as a green-emitting phosphor for white LEDs. In addition, the luminescence of Yb^{2+} is quenched at much lower temperature than the Eu^{2+}-doped samples. This can be evidenced by the emission intensity of Ca_2PO_4Cl:Yb^{2+} at 100 °C which drops off 40% of its initial value at room temperature and remains at only 20% of its initial value when the temperature was raised up to 250 °C whereas the emission intensity of the Ca_2PO_4Cl:Eu^{2+} at 250 °C still maintains about 75% of its initial value at room temperature. From the observation of the contrasting thermal quenching behaviors between Yb^{2+} and Eu^{2+} in Ca_2PO_4Cl, along with the much broader Yb^{2+} emission than Eu^{2+} emission, we concluded that the lowest 5d state of Yb^{2+} at both Ca sites is located within the conduction band while the lowest 5d state of Eu^{2+} is located below the conduction band. Yb^{2+} is prone to be photoionized than Eu^{2+} in the same host possibly due to the fact that the divalent state for Yb^{2+} is less stable than that of Eu^{2+} as evidenced by the ease of oxidation of Yb^{2+} compared to Eu^{2+} in acidic solution [25,26], and the standard redox potential of Yb^{3+}(aq)/Yb^{2+}(aq) (−1.15 V) is smaller than that of Eu^{3+}(aq)/Eu^{2+}(aq) (−0.43 V) [25,26]. In addition, it can be seen from Fig. 5(a), for the Yb^{2+}-doped sample, the two Gaussian emission bands quench differently. In particular, the emission band at 450 nm is nearly quenched at 100 °C. As a result, when the temperature is increased above 100 °C, the peak shape of PL spectrum transforms from asymmetric to symmetric. As described previously, the two different Ca^{2+} sites available for Yb^{2+} to occupy in Ca_2PO_4Cl:Yb^{2+} may produce two different Yb^{2+}-trapped exciton states. The emission band at 450 nm is from the de-excitation of the Yb^{2+}-trapped exciton state with a higher energy while the emission band at 495 nm results from the de-excitation of the Yb^{2+}-trapped exciton state with a lower energy. With increasing of temperature, the probability of nonradiative transition from the higher energy to lower energy Yb^{2+}-trapped exciton state increases; thus, as a consequence, the Gaussian emission band at 450 nm quenches relatively fast as compared to the emission band at 495 nm.

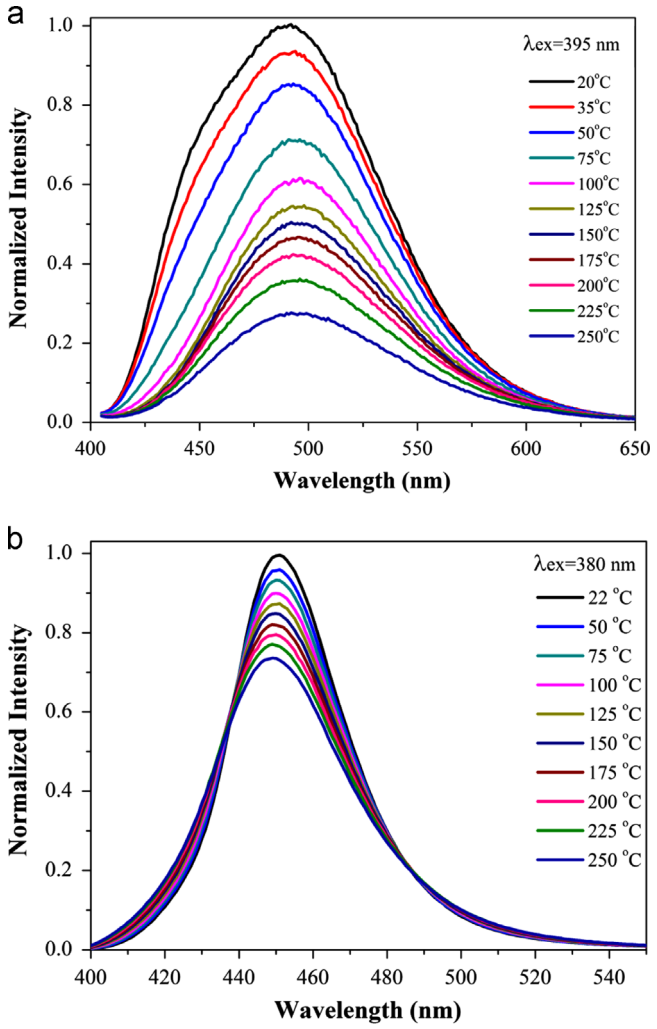

Fig. 5. Dependence of PL intensity on temperature for (a) $Ca_2PO_4Cl:2\%Yb^{2+}$ and (b) $Ca_2PO_4Cl:2\%Eu^{2+}$.

3.4. Comparision of luminescence performance between $Ca_2PO_4Cl:Yb^{2+}$ and $BaSi_2O_2N_2:Eu^{2+}$

In order to evaluate the applicability of $Ca_2PO_4Cl:Yb^{2+}$ for fabrication of white-light LED, we have compared the PL intensity and external quantum efficiency (EQE) of $Ca_2PO_4Cl:Yb^{2+}$ with those of $BaSi_2O_2N_2:Eu^{2+}$ (ZYP500N, from Beijing Nakamura-Yuji Science and Technology Co., Ltd.). Shown in Fig. 6 are the PL spectra of $Ca_2PO_4Cl:3\%Yb^{2+}$ and $BaSi_2O_2N_2:Eu^{2+}$ under 395 nm excitation. The results show that the integrated PL intensity from 410 nm to 600 nm range for $Ca_2PO_4Cl:3\%Yb^{2+}$ is 30% of that for $BaSi_2O_2N_2:Eu^{2+}$. The optical absorbance and EQE, which were calculated by using the method previously reported by de Mello et al. [27], were found to be 51% and 24% for $Ca_2PO_4Cl:3\%Yb^{2+}$, and 82% and 71% for $BaSi_2O_2N_2:Eu^{2+}$, respectively. In view of the low quantum efficiency and considerable thermal quenching, $Ca_2PO_4Cl:Yb^{2+}$ is presumably unsuitable for use in the fabrication of white-light LEDs.

4. Conclusions

In summary, the luminescence properties of Yb^{2+} in Ca_2PO_4Cl were investigated as an alternate to Eu^{2+}. The Yb^{2+}-activated Ca_2PO_4Cl shows green emission resulting from the de-excitation of the impurity Yb^{2+}-trapped exciton state. The low-temperature emission spectrum of Yb^{2+} doped Ca_2PO_4Cl indicates there are two kinds

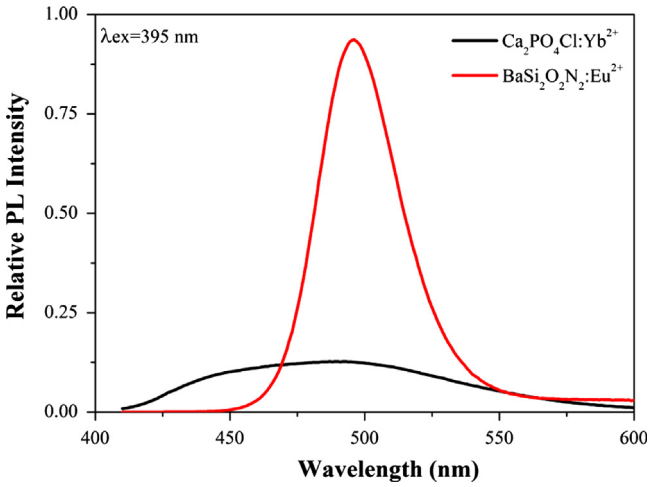

Fig. 6. PL spectra of $Ca_2PO_4Cl:3\%Yb^{2+}$ and $BaSi_2O_2N_2:Eu^{2+}$ (ZYP500N) upon 395 nm excitation.

of Yb^{2+} emission centers in Ca_2PO_4Cl. The emission from Yb^{2+} located at the larger Ca^{2+} site is responsible for the emission at 450 nm while that at the small Ca^{2+} site is responsible for the emission at 495 nm. Due to the thermal-assisted energy transfer between the two luminescent centers, the emission band at 450 nm quenches much faster than that at 495 nm. In addition, we have compared the luminescence of Yb^{2+}- and Eu^{2+}-doped Ca_2PO_4Cl. Our results suggest that Yb^{2+} luminescence is significantly different from that of Eu^{2+}, characterized by a much broader FWHW and a lower quenching temperature. Based on the similar findings of previous studies on solely Yb^{2+}-doped materials, we suggest that the lowest 5d state of Yb^{2+} is located within the conduction band of the host while that of Eu^{2+} is located below the conduction band of Ca_2PO_4Cl. Because of the low quantum efficiency and considerable thermal quenching, Yb^{2+}-doped Ca_2PO_4Cl is presumably unsuitable for use in phosphor-converted white LED.

Acknowledgment

This work was supported by the National Science Council under Contract numbers NSC100-2811-M-009-068 (D.-Y.W.) and NSC101-2113-M-009-021-MY3 (T.-M.C.).

Appendix A. Supporting information

Supplementary data associated with this article can be found in the online version at http://dx.doi.org/10.1016/j.jlumin.2013.11.082.

References

[1] W.B. Im, S. Brinkley, J. Hu, A. Mikhailovsky, S.P. DenBaars, R. Seshadri, Chem. Mater. 22 (2010) 2842.
[2] S.E. Brinkley, N. Pfaff, K.A. Denault, Z.J. Zhang, H.T. Hintzen, R. Seshadri, S. Nakamura, S.P. DenBaars, Appl. Phys. Lett. 99 (2011) 241106.
[3] V. Bachmann, C. Ronda, A. Meijerink, Chem. Mater. 21 (2009) 2077.
[4] M. Zeuner, P.J. Schmidt, W. Schnick, Chem. Mater. 21 (2009) 2467.
[5] K. Kimoto, R.J. Xie, Y. Matsui, K. Ishizuka, N. Hirosaki, Appl. Phys. Lett. 94 (2009) 041908.
[6] C. Hecht, F. Stadler, P.J. Schmidt, V. Baumann, W. Schnick, Chem. Mater. 21 (2009) 1595.
[7] D.Y. Wang, C.H. Huang, Y.C. Wu, T.M. Chen, J. Mater. Chem. 21 (2011) 10818.
[8] C.J. Duan, A. Delsing, H.T. Hintzen, Chem. Mater. 21 (2009) 1010.
[9] V. Bachmann, C. Ronda, O. Oeckler, W. Schnick, A. Meijerink, Chem. Mater. 21 (2009) 316.
[10] C.H. Huang, W.R. Liu, T.M. Chen, J. Phys. Chem. C 114 (2010) 18698.
[11] Q. Li, N. Hirosaki, R.J. Xie, T. Takeda, M. Mitomo, Chem. Mater. 20 (2008) 6704.

[12] X.Q. Piao, K. Machida, T. Horikawa, H. Hanzawa, Y. Shimomura, N. Kijima, Chem. Mater. 19 (2007) 4592.
[13] Y.C. Chiu, W.R. Liu, C.K. Chang, C.C. Liao, Y.T. Yeh, S.M. Jang, T.-M. Chen, J. Mater. Chem. 20 (2010) 1755.
[14] H.S. Yoo, S. Vaidyanathan, S.W. Kim, D.Y. Jeon, Opt. Mater. 31 (2009) 1055.
[15] Y. Huang, P. Wei, S. Zhang, H.J. Seo, J. Electrochem. Soc. 158 (2011) H465.
[16] Z. Zhang, O.M. ten Kate, A.C. Delsing, M.J.H. Stevens, J. Zhao, P.H.L. Notten, P. Dorenbos, H.T. Hintzen, J. Mater. Chem. 22 (2012) 23871.
[17] L.H. Liu, R.J. Xie, N. Hirosaki, T. Takeda, C.N. Zhang, J.G. Li, X.D. Sun, Sci. Technol. Adv. Mater. 12 (2011) 034404.
[18] P. Dorenbos, J. Lumin. 104 (2003) 239.
[19] F.C. Palilla, B.E. Oreilly, V.J. Abbruscato, J. Electrochem. Soc. 117 (1970) 87.
[20] M. Greenblatt, E. Banks, B. Post, Acta Crystallogr. 23 (1967) 166.
[21] P.D. Rack, P.H. Holloway, Mater. Sci. Eng. R 21 (1998) 171.
[22] D.S. McClure, C. Pedrini, Phys. Rev. B 32 (1985) 8465.
[23] V. Bachmann, T. Justel, A. Meijerink, C. Ronda, P.J. Schmidt, J. Lumin. 121 (2006) 441.
[24] V. Bachmann, A. Meijerink, C. Ronda, J. Lumin. 129 (2009) 1341.
[25] S. Lizzo, E.P. Nagelvoort, R. Erens, A. Meijerink, G.J. Blasse, Phys. Chem. Solids 58 (1997) 963.
[26] G. Singh, Chemistry of Lanthanides and Actinides, Discovery Publishing House, New Delhi (2007) 12.
[27] J.C. de Mello, H.F. Wittmann, R.H. Friend, Adv. Mater. 9 (1997) 230.